Mass systematics of evaporation residues from ^{35}Cl- and ^{32}S-induced fusion on light targets*

T. M. Cormier,† E. R. Cosman, and A. J. Lazzarini
Department of Physics and Laboratory for Nuclear Science, Massachusetts Institute of Technology, Cambridge, Massachusetts 02139

H. E. Wegner and J. D. Garrett‡
Brookhaven National Laboratory,† Upton, New York 11973

F. Pühlhofer§
Gesellschaft für Schwerionenforschung mbH, Darmstadt, Germany
(Received 25 August 1976)

Evaporation residues of reactions between ^{24,25,26}Mg, ^{27}Al, and ^{28}Si as targets and 100–170 MeV ^{35}Cl and 130 MeV ^{32}S beams and also between ^{28}Si and 117.5 MeV ^{28}Si ions were measured at small forward angles using a time-of-flight telescope. The mass distributions of the products show a complex structure, which is shown to vary smoothly with beam energy and target mass. A dominant decay mode of the compound nucleus can be assigned to each residue mass using the shape of the angular distribution. An evaporation model calculation predicts qualitatively the main features of the mass distributions.

[NUCLEAR REACTIONS ^{35}Cl + ^{24,25,26}Mg, ^{28}Si fusion, E = 145.6 MeV. ^{35}Cl + ^{27}Al fusion, E = 100, 110, 120, 130, 140, 145.6, 170 MeV; $\sigma(\theta)$ at 170 MeV. ^{32}S + ^{24,25,26}Mg, ^{27}Al, ^{28}Si fusion, E = 130 MeV; $\sigma(\theta)$ for ^{32}S + ^{27}Al. ^{28}Si + ^{28}Si fusion, E = 117.5 MeV. Comparison of mass distribution of evaporation residues with statistical particle evaporation calculations.]

I. INTRODUCTION

Recent experimental measurements[1] of heavy ion reactions have concentrated on total cross sections for a particular process (e.g., fusion, "deep inelastic," etc.) as a function of energy and angular momentum. The development of detection techniques adequate to distinguish the details of the mass and/or charge distribution of reaction products, allows the study of the particle decay of the composite system (see, e.g., Refs. 2–6).

The present paper reports data on the mass systematics of the evaporation residues produced in the bombardment of ^{24,25,26}Mg and ^{28}Si targets with 145.6 MeV ^{35}Cl ions, a ^{27}Al target with 100–170 MeV ^{35}Cl ions, ^{24,25,26}Mg, ^{27}Al, and ^{28}Si targets with 130 MeV ^{32}S ions, and a ^{28}Si target with 117.5 MeV ^{28}Si ions. The structure observed in the mass distribution of the evaporation residues reflects the competition between α-particle and nucleon (proton and neutron) evaporation in the deexcitation of the composite system. Such mass systematics can be reproduced qualitatively by statistical calculations of multiple particle emission from the fused system.

II. EXPERIMENTAL PROCEDURE

The three-stage tandem facility of Brookhaven National Laboratory was used to provide the various energy ^{35}Cl, ^{32}S, and ^{28}Si ions as well as the electronic equipment and computer facilities for data acquisition and analysis. Foils of ≈100 μg/cm^2, ^{24,25,26}Mg and ^{28}Si enriched to >98% and on thin C backings and a 75 μg/cm^2 self-supporting natural Al foil were used for targets. The ^{35}Cl + ^{27}Al angular distribution and excitation function data, however, were obtained with an 800 μg/cm^2 self-supporting natural Al target.

The basic experimental method has been described previously.[2,7] Briefly, the mass identification was accomplished with a time-of-flight (TOF) system consisting of a thin scintillator start detector followed by a silicon-surface-barrier stop detector at the end of a flight path of approximately 2 m. Reductions in the efficiency of such a system, due to multiple scattering in the scintillator foil, are negligibly small for the exiting energies of the evaporation residues in the present work. The mass and energy calibration of the basic data was accomplished by the elastic scattering of ^{51}V and ^{56}Fe ions.

A typical variable density mass vs laboratory energy plot for 145.6 MeV ^{35}Cl incident on ^{27}Al is shown in Fig. 1. The mass scale is provided by the analog multiplication of the fusion fragment energy E by the time-of-flight, squared, t^2. The mass lines in the vicinity of a particular fusion region were sufficiently parallel to warrant a simple energy sum on the mass axis for detailed analysis. The yield of the evaporation residues as a function of mass were then extracted using a multipeak

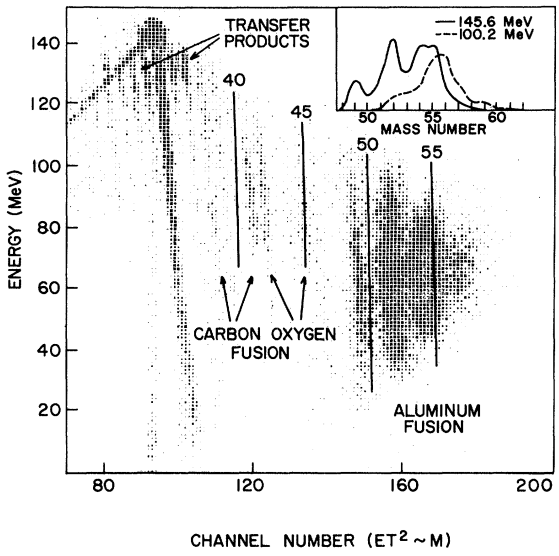

FIG. 1. Variable density plot of $Et^2 \simeq M$ data for 145.6 MeV ^{35}Cl ions incident on ^{27}Al at 7.2° (lab). The varying size point indicates counts per channel on a scale of 1 to 20 counts. Each full square point indicates ≥ 20 counts. The oxygen and carbon contaminent fusion regions are indicated. The inset shows the mass projection for the ^{35}Cl + ^{27}Al region. The corresponding mass spectrum for 100 MeV ^{35}Cl is also shown for comparison.

Gaussian fit to these mass distributions. The error flags shown with the data reflect statistical uncertainties as well as an estimate of the errors from the data analysis.

III. EXPERIMENTAL RESULTS

The systems studied are summarized in Table I, and the compound system, incident energy, and angular dependence of the yield of the evaporation residues as a function of mass are discussed in subsections A, B, and C, respectively.

A. Mass distribution dependence on compound system

The mass distributions of evaporation residues at the scattering angle of 7.2° (lab) for the fusion of 145.6 MeV ^{35}Cl ions and 130 MeV ^{32}S ions with ^{24,25,26}Mg, ^{27}Al, and ^{28}Si are shown in Figs. 2 and 3. In these figures the highest peaks of each mass distribution are approximately normalized in order to emphasize the similarities and differences in mass distribution. The 7.2° laboratory angle was chosen because the relative mass distribution at that angle is similar to that of the total integrated cross section — see Fig. 4.

The similarity of the differential mass distributions of the evaporation residues for the same projectile on the ^{25,26}Mg, ^{27}Al, and ^{28}Si targets is

TABLE I. Summary of reactions studied.

Incident system	Compound nucleus	Incident energy (MeV) lab	c.m.	Excitation of compound system (MeV)	Ang. dist.
^{28}Si + ^{28}Si	^{56}Ni	117.5	58.75	69.67	No
^{32}S + ^{24}Mg	^{56}Ni	130	55.71	69.67	No
^{32}S + ^{25}Mg	^{57}Ni	130	57.02	73.92	No
^{32}S + ^{26}Mg	^{58}Ni	130	58.28	76.29	No
^{32}S + ^{27}Al	^{59}Cu	130	59.49	72.64	Yes
^{32}S + ^{28}Si	^{60}Zn	130	60.67	67.36	No
^{35}Cl + ^{24}Mg	^{59}Cu	145.6	59.23	75.65	No
^{35}Cl + ^{25}Mg	^{60}Cu	145.6	60.67	76.82	No
^{35}Cl + ^{26}Mg	^{61}Cu	145.6	62.06	78.82	No
^{35}Cl + ^{27}Al	^{62}Zn	100	43.55	58.46	No
		110	47.90	62.81	No
		120	52.26	67.17	No
		130	56.61	71.53	No
		140	60.97	75.88	No
		145.6	63.41	78.32	No
		170	74.03	88.94	Yes
^{35}Cl + ^{28}Si	^{63}Ga	145.6	64.71	70.93	No

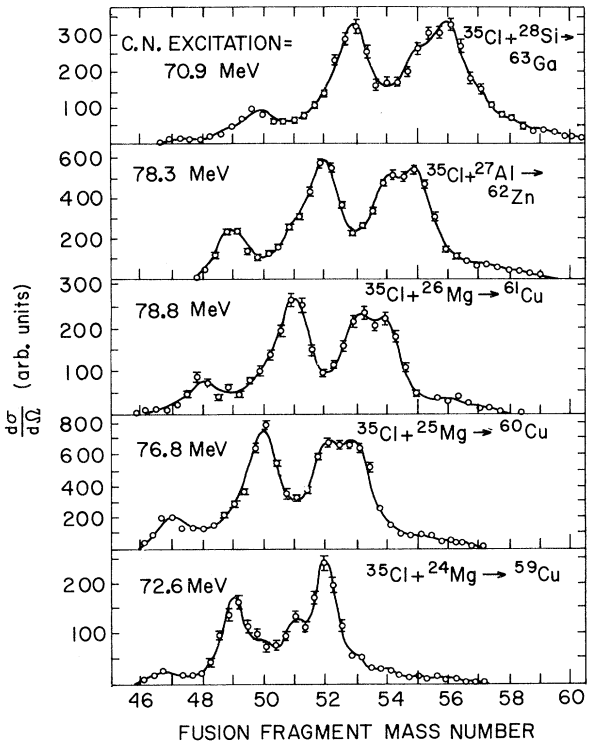

FIG. 2. Evaporation residue mass distributions for 145.6 MeV ^{35}Cl ions incident on ^{28}Si, ^{27}Al, and ^{26,25,24}Mg at 7.2° (lab). The compound nucleus excitation for the fused system is indicated for each case. The solid line is a multipeak Gaussian least square fit to the data.

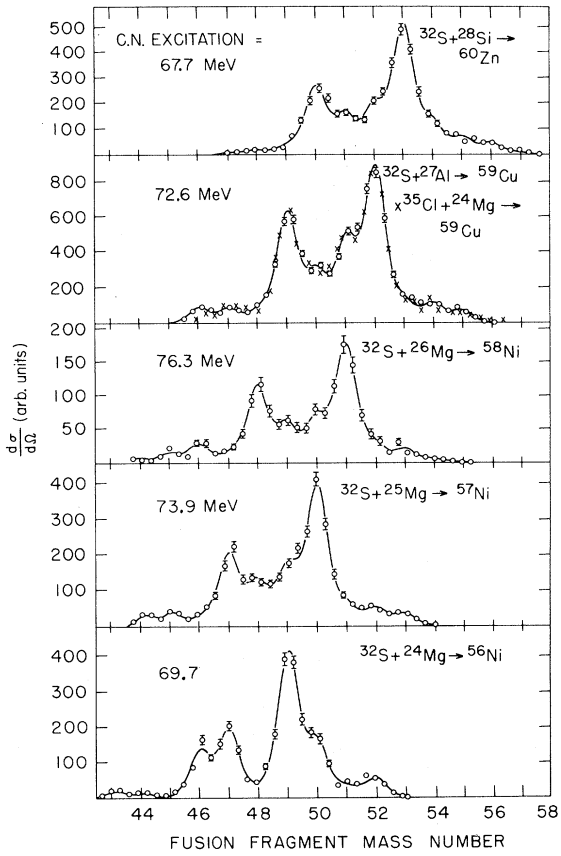

FIG. 3. Evaporation residue mass distributions for 130 MeV ^{32}S ions incident on ^{28}Si, ^{27}Al, and ^{26,25,24}Mg at 7.2° (lab). Compound nucleus excitation for the fused system is indicated for each case. The ^{35}Cl+ ^{24}Mg fusion data from Fig. 2 is superimposed for comparison with the ^{32}S+^{27}Al data which populate the same compound system. The solid line is a multipeak Gaussian least square fit to the data.

striking (see Figs. 2 and 3). However, both in the ^{35}Cl and in the ^{32}S data the shape of the mass distribution for the ^{24}Mg target deviates from that observed for the other isotopes. The same ^{59}Cu compound system is formed by ^{35}Cl+^{24}Mg and ^{32}S+^{27}Al. For 145.6 MeV ^{35}Cl and 130 MeV ^{32}S, the compound system is formed at the same excitation energy and with nearly the same grazing angular momentum. Hence the ^{35}Cl+^{24}Mg and the ^{32}S+^{27}Al differential mass data are nearly identical (see Fig. 3), as expected, even though the ^{35}Cl+^{24}Mg data deviates from similar mass distribution for ^{35}Cl on the other targets.

Data also were obtained for ^{28}Si+^{28}Si at an incident energy of 117.8 MeV which populates the ^{56}Ni compound system at the same excitation energy as 130 MeV ^{32}S+^{24}Mg. The differential mass distributions measured at a laboratory angle of 7.2° for these two systems are compared in Fig. 5. The "shape" of the measured mass distributions is nearly the same within the experimental errors, even though, for identical projectile and target (^{28}Si+^{28}Si) the compound system is formed only with even angular momentum.

B. Energy dependence of mass distribution

The energy dependence of the fusion product mass distribution at 7.2° (lab) for the fusion of 100–170 MeV ^{35}Cl with ^{27}Al is shown in Fig. 6. A gradual shift of the mass distribution to lighter masses with increasing energy is observed with a decrease of 2 mass units for the predominant mass groups for a change of compound nucleus excitation energy from 58.5 to 88.9 MeV. This corresponds

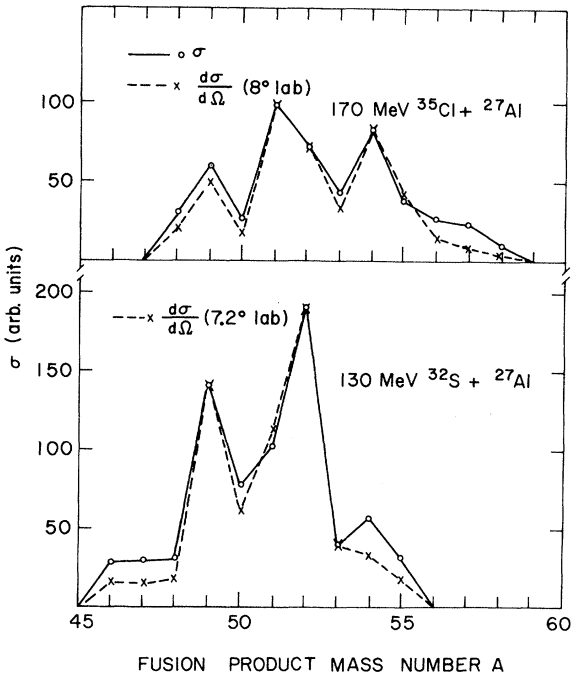

FIG. 4. A shape comparison of differential cross section $d\sigma/d\Omega$ and total cross section σ for 170 MeV $^{35}Cl + ^{27}Al$ at 8° (lab) and 130 MeV $^{32}S + ^{27}Al$ at 7.2° (lab). The σ and $d\sigma/d\Omega$ scales have been normalized arbitrarily at the maximum cross sections. If an appropriate forward angle is chosen the shape comparison with the total angle integrated cross section is quite good.

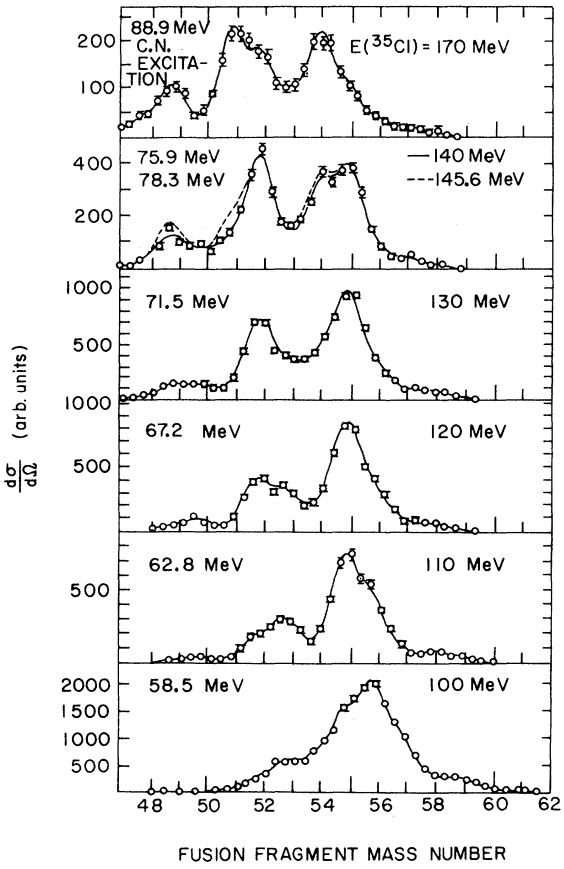

FIG. 6. Energy dependence of the evaporation residue mass distributions for 100–170 MeV $^{35}Cl + ^{27}Al$ fusion at 7.2° (lab). The compound nucleus excitation for the fused system is indicated in each case. The solid line is a multipeak Gaussian least square fit to the data.

to ~15 MeV/mass unit. Also at higher compound nucleus excitation energies more strength is distributed to the lighter mass groups, corresponding to increased α-particle emission. Even an increase as small as 2.4 MeV in the excitation of the compound system produces a detectable shift to lighter masses (see Fig. 6). At the highest incident energy, 170 MeV, $^{35}C + ^{27}Al$ data fissionlike cross sections were observed to compete with light particle emission in the decay of the compound system.[8]

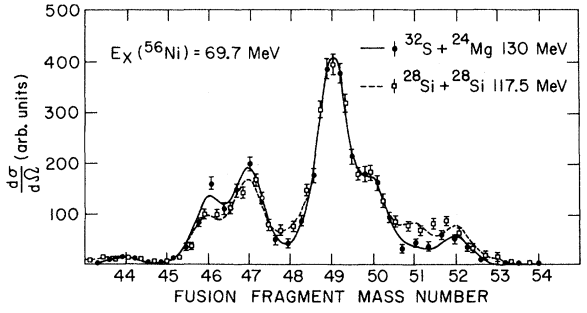

FIG. 5. Evaporation residue mass distribution comparison for 130 MeV ^{32}S ions incident on ^{24}Mg and 117.5 MeV ^{28}Si ions incident on ^{28}Si at 7.2° (lab).

C. Angular dependence of the mass distribution

The angular dependence of the evaporation residue mass distributions corresponding to 170 MeV ^{35}Cl and 130 MeV ^{32}S on ^{27}Al are shown in Figs. 7 and 8 and the corresponding angular distributions are shown in Figs. 9 and 10. The angular distributions corresponding to the heaviest mass residues are sharply forward peaked for both ^{35}Cl and ^{32}S projectiles. At mass 55 for the

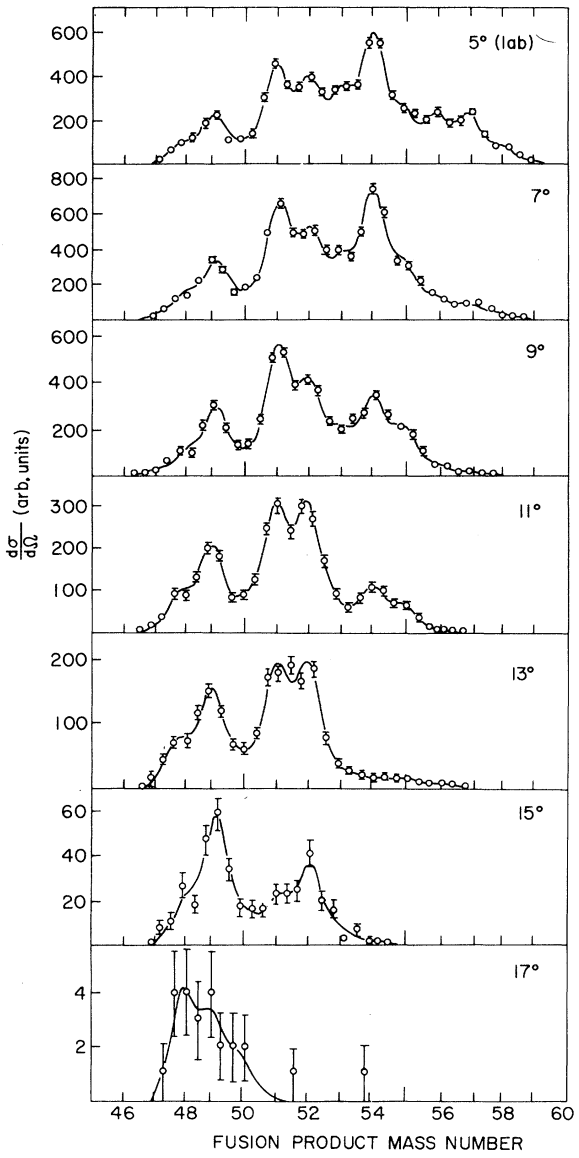

FIG. 7. Angular dependence of evaporation residue mass distributions for 170 MeV $^{35}Cl + ^{27}Al$. The solid lines are multipeak Gaussian fits to the data used to extract the strength of individual masses.

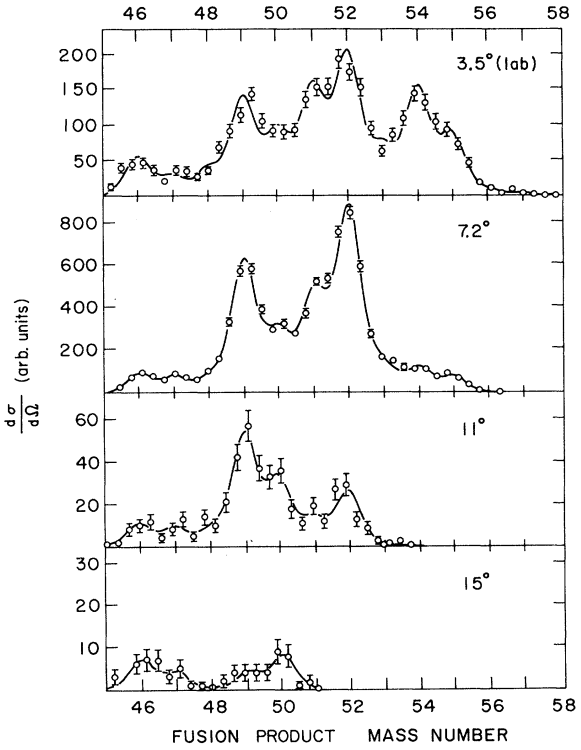

FIG. 8. Angular dependence of the evaporation residue mass distributions for 130 MeV $^{32}S + ^{27}Al$. The solid lines are multipeak Gaussian fits to the data used to extract the strength of individual masses.

^{35}Cl data and mass 53 for the ^{32}S data there is a marked change in the angular distributions from sharply forward peaked to level or even to a decrease in yield at forward angles. This change in the angular shape is attributed to the increased role of α emission in the formation of the lighter mass residues. Isotropic evaporation of nucleons does not produce much transverse momentum and consequently the resulting heavier mass particles are strongly peaked forward. However, the evaporation of an α particle can produce appreciable transverse momentum. In fact, the solid angle for evaporation in the forward and backward direction, which allows the fusion product to continue in the forward direction, is small compared to the rest of the solid angle that results in larger scattering angles. Consequently, those fusion products formed by α evaporation are less likely to be found at 0° than at some finite scattering angle. Similarly, evaporation residues formed by two and three α-particle evaporations should be found with comparable probability at even larger angles as observed.

IV. COMPARISON WITH EVAPORATION CALCULATIONS

The reactions reported in this work are interpreted as fusion reactions. It is assumed that the projectile and target nucleus form a highly

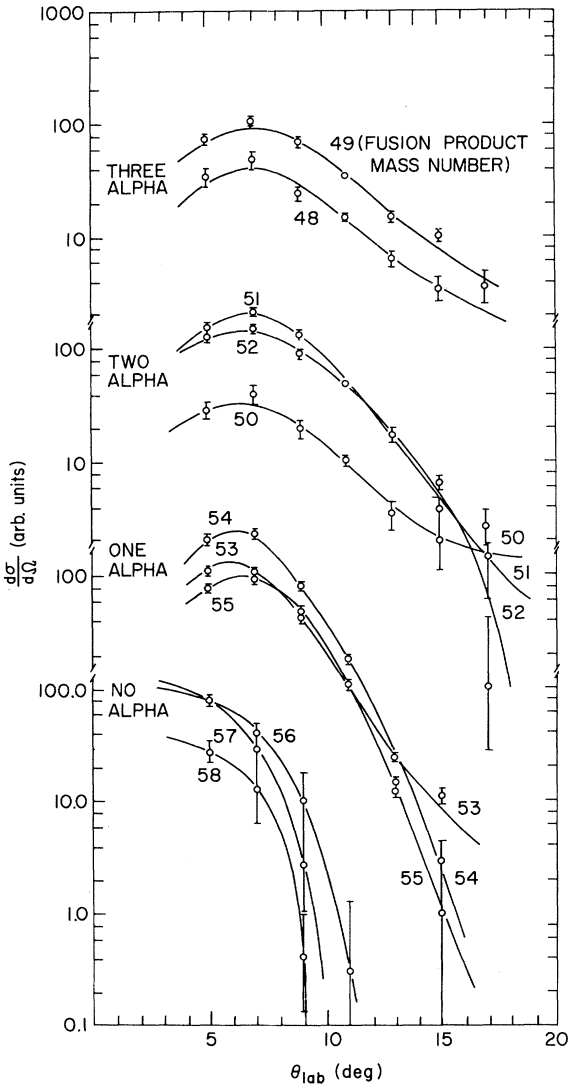

FIG. 9. Angular distributions of individual evaporation residue masses for 170 MeV ^{35}Cl ions incident on ^{27}Al. The various mass groups are offset vertically for clarity. Error bars are determined by the multipeak fitting program. The solid lines are to guide the eye. Proposed α-particle evaporation corresponding to the different mass groups are indicated.

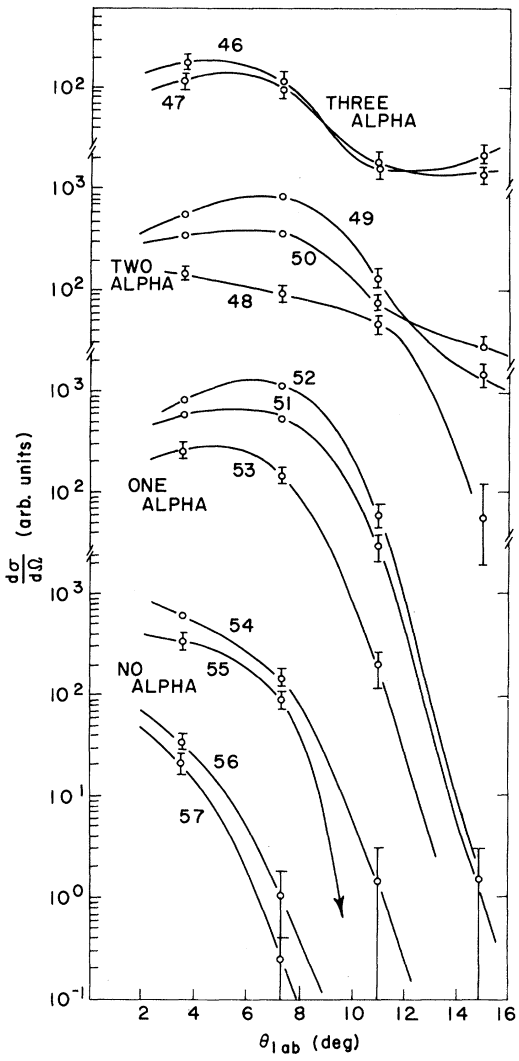

FIG. 10. Angular distributions of individual fusion product masses for 130 MeV ^{32}S ions incident on ^{27}Al. The various mass groups are offset vertically for clarity. The error bars are determined from the multipeak fitting program. The solid lines are to guide the eye. Proposed α-particle evaporation corresponding to the different mass groups are indicated.

excited compound nucleus, which emits a number of light particles until the excitation energy has decreased sufficiently so that it only can deexcite further by γ rays. The evaporation residue mass distributions, which are the main results of this study, reflect the intensity of the various decay chains. It has been noted previously that their structure arises from the competition between nucleon emission and α decay.[2,5]

Assuming statistical equilibrium, the decay of the compound system can be calculated from the Hauser-Feshbach theory. This was done using the nuclear evaporation code CASCADE.[9] The code is organized such that all possible decay sequences available for neutron, proton, α-particle, and γ-ray emission are followed automatically until the

excitation energy is below the particle thresholds. The calculation will be described extensively in a subsequent publication.[9] The parameters, therefore, are mentioned only briefly in the following paragraphs.

The initial spin distribution in the compound nucleus was calculated on the basis of a strong-absorption model from the fusion cross sections measured by Gutbrod *et al.*[10] using the same diffuseness as that obtained from the optical model[10] for the reaction cross section. For example, the initial spin distribution assumed for 170 MeV ^{35}Cl + ^{27}Al is shown in Fig. 11. Branching ratios for the above-mentioned particle decays are determined by the level densities in the final nuclei and the corresponding transmission coefficients. The latter were calculated from average optical potentials given in the literature.[11] The results are not very sensitive to the parameter set used, since the compound-nucleus excitation, and hence the decay energies, are relatively high. γ decay was treated as described by Grover and Gilat,[12] using reduced decay widths for $E1$, $M1$, and $E2$ transitions as obtained from lifetimes of low-lying states. The parameters for γ decay can usually be altered by an order of magnitude without a significant change in the evaporation residue results.

The parameters for the level densities, on the other hand, must be determined very carefully. For the analytical form of the level density Lang's formula was used, as cited by Gilat and Grover.[13] The parameters a (level density parameter) and Δ (shift of the virtual compared with the actual ground state) were taken from the work of Dilg, Schantl, and Vonack.[14] The values given there were used for determining the parameters for interpolation formulas, which contain a smooth background as function of A and shell effects in the vicinity of shell closures ($Z = 28$ and $N = 28$). Near the ground state some levels were inserted, e.g., in an even-even nucleus a $0^+, 2^+, 4^+, 6^+$ sequence with average excitation energies. At high excitation energy ($E_x \geq 20$ MeV) it was assumed that the nuclei behave as predicted by the liquid-drop theory, i.e., the parameter a was set constant ($A/8$ MeV) and Δ was chosen so that the virtual ground state for the level densities coincided with that of a spherical liquid drop as calculated from the Myers-Swiatecki mass formula[15] without shell and pairing corrections. The spin dependence of the level densities is parametrized using an effective moment of inertia, which also determines the shape of the yrast line. At high excitation energy this was taken to be equal to that of a deformable liquid drop with the radius parameter $r_0 = 1.27$ fm (Ref. 16) for the sphere. The magnitude of the deformation at higher angular momenta was taken from the work of Cohen, Plasil, and Swiatecki.[17] The effective moment of inertia was gradually reduced by 15% at lower excitation energies. The resulting yrast line for $A = 60$ is shown in Fig. 11.

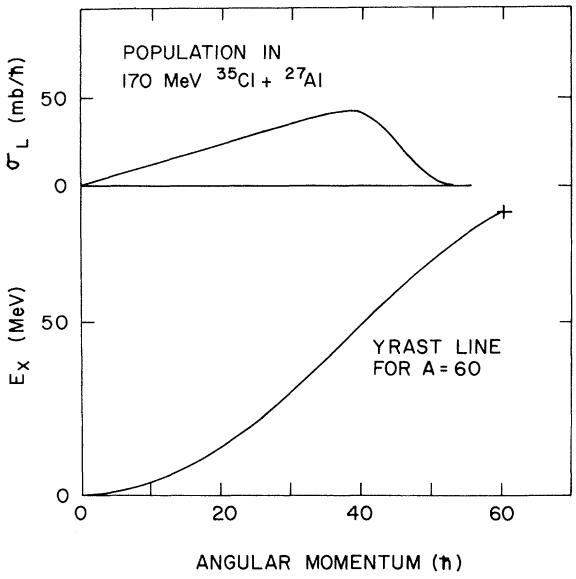

FIG. 11. Yrast line for a nucleus with $A = 60$ calculated from the rotating-liquid-drop model (Ref. 17). For comparison, the spin distribution assumed for the compound nucleus of the reaction 170 MeV ^{35}Cl on ^{27}Al is shown at the appropriate excitation energy.

The comparison between calculated and experimental mass distributions is shown in Fig. 12 for the two cases where angle-integrated cross sections have been obtained. In both cases the complicated structure of the mass distribution is reproduced. Calculations for the other systems investigated also were performed with exactly the same parameters and compared with the differential cross section data in Fig. 13. The steep slope of the fusion product angular distributions distorts the heavy end of the mass distribution as shown in a comparison of differential and total cross section (Fig. 4) and again indicated in this comparison. It is observed, however, that the systematic shift of the peaks for different targets as well as relative intensity changes including the somewhat unexpected differences in the shape of the mass distributions for ^{24}Mg are qualitatively reproduced. It is interesting to note the difference in the prediction for the two reactions leading to the same compound nucleus at the same excitation, ^{35}Cl + ^{24}Mg and ^{32}S + ^{27}Al. The experimental agreement is striking (Fig. 3); however, the comparison is for differential cross section, not total as the calculations.

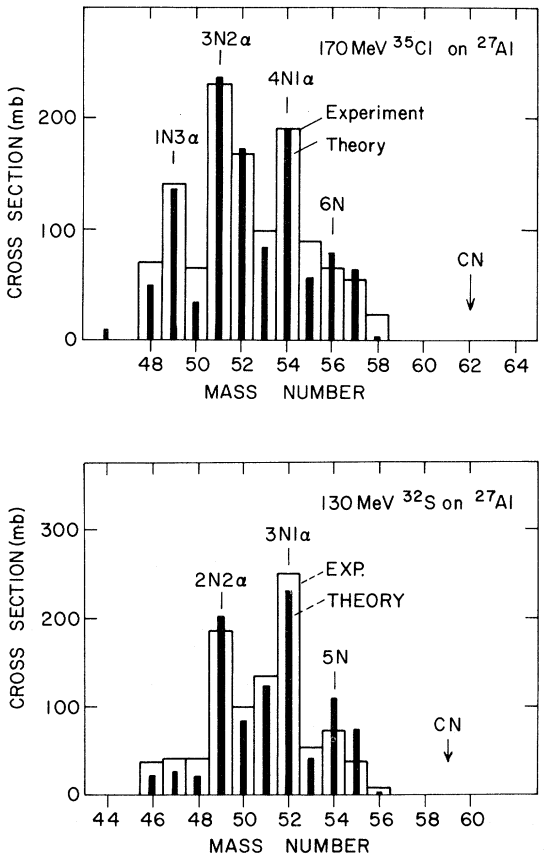

FIG. 12. Comparison of angle integrated experimental cross sections with the predictions of CASCADE for 170 MeV ^{35}Cl + ^{25}Al and 130 MeV ^{32}S + ^{27}Al. The absolute cross section scale of Ref. 10 has been used for the experimental data.

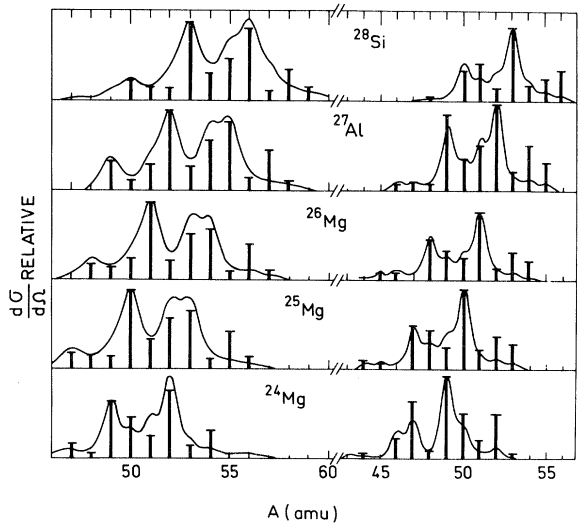

FIG. 13. Shape comparison of the differential cross sections of Figs. 2 and 3 with the total cross section predictions of CASCADE. The comparisons in each case are made by normalizing the predictions to the most predominant peak in the experimental data.

It is suggested in Sec. III that the number of emitted α particles can be inferred from the shape of the angular distribution. It is possible to check this assumption by comparison with the calculations. Table II shows the number of evaporated particles corresponding to each evaporation residue mass for the 170 MeV ^{35}Cl + ^{27}Al data. For each mass group the different possible decay sequences are given together with the corresponding predicted cross section in millibarns. Decay routes having a predicted cross section of < 1 mb are suppressed in the table. For A = 56–58 multinucleon decay is predicted to dominate the cross section in agreement with the sharply forward peaked angular distributions (see Fig. 9 and the discussion in Sec. III). For A = 55 three-α nucleon decay is predicted to dominate the cross section in agreement with the broadened angular distribution. Similarly, the transition from single- to two-α emission is predicted and observed between A = 53 and 52, and the transition from two-α to three-α emission is predicted and observed between A = 51 and 49.

It is emphasized that the parameters have not been individually adjusted in these calculations. Instead it was tried to fit all experimental mass distributions with the same average parameters.

Calculations indicate that including discrete levels near the ground state (i.e., below the excitation, Δ, where the continuous level densities start) is important in reproducing the magnitude of the α-particle decay. The large contribution from α-particle evaporation can be understood by considering the angular momentum relations for 170 MeV ^{35}Cl or ^{27}Al (Fig. 9). In this mass region, where the Coulomb barrier for α emission is sufficiently low, γ decay cannot seriously compete with particle emission above the particle threshold even near the yrast line. Thus on the average about 30$\hbar$ of angular momentum are available to be carried away by the four to six particles emitted.

In such fusion reactions, many nuclei with high spin and excitation are involved during the deexcitation process of the compound nucleus. It is expected that a new understanding of such nuclear systems may be gained through detailed compari-

TABLE II. Calculated evaporation scheme for the compound nucleus ^{62}Zn formed at an excitation of 88.9 MeV by the reaction of 170 MeV ^{35}Cl on ^{27}Al. ( ) denotes calculated cross section in mb (if ≥1 mb).

A_R [a]	Number of emitted particles 3	4	5	6	7	Total yield (mb)
58		$3p1n$(2)				2
57			$2p3n$(3) $3p2n$(47) $4p1n$(13)			64
56				$3p3n$(40) $4p2n$(38)		79
55		$1\alpha1p2n$(3) $1\alpha2p1n$(42) $1\alpha3p$(8)			$3p4n$(1) $4p3n$(2)	56
54			$1\alpha1p3n$(2) $1\alpha2p2n$(72) $1\alpha3p1n$(115)			190
53	$2\alpha1p$(9)			$1\alpha2p3n$(15) $1\alpha3p2n$(58)		84
52		$2\alpha2p$(2) $2\alpha1p1n$(103) $2\alpha2n$(66)			$1\alpha3p3n$(1)	172
51			$2\alpha1p2n$(34) $2\alpha2p1n$(191) $2\alpha3p$(11)			236
50	3α(13)			$2\alpha2p2n$(9) $2\alpha3p1n$(11)		33
49		$3\alpha1n$(34) $3\alpha1p$(103)				137
48			$3\alpha1p1n$(46) $3\alpha2p$(4)			50
47						<1
46		4α(11)				11

[a] A_R denotes fusion product mass number.

sons of calculation and experiment over various regions of the Periodic Table. It would be desirable, however, to obtain not only mass but also element distributions from the experiment. Such measurements are just now becoming possible in the mass region discussed in this paper.

We should like to acknowledge the assistance of J. D. Larson in preparing the Gaussian fitting routine.

*Work performed under the auspices of the U. S. Energy Research and Development Administration.

†Present address: Physics Department, State University of New York, Stony Brook, New York.

‡Present address: Niels Bohr Institute, University of Copenhagen, DK2100 Copenhagen Ø, Denmark.

§On leave from: Fachbereich Physik der Universitat Marburg, Germany.

[1]See the review papers given at recent heavy-ion conferences, e.g., in *Proceedings of the Symposium on Classical and Quantum Mechanical Aspects of Heavy Ion Collisions, Heidelberg, Germany, October 1974,* edited by H. L. Harney *et al.* (Springer, Berlin, 1975); in *Proceedings of the International Conference on Reactions between Complex Nuclei, Nashville, 1974,* edited by R. L. Robinson *et al.* (North-Holland, Amster-

dam/American Elsevier, New York, 1974), Vols. I and II; in *Proceedings of the Third International Symposium of the Physics and Chemistry of Fission, Rochester, 1973* (International Atomic Energy Agency, Vienna, 1974), Vol. II.

[2]J. D. Garrett, H. E. Wegner, T. M. Cormier, E. R. Cosman, and A. J. Lazzarini, Phys. Rev. C 12, 481 (1975).

[3]R. Broda, M. Ishihara, B. Herskind, H. Oeschler, S. Ogaza, and H. Ryde, Nucl. Phys. A248, 356 (1975).

[4]R. Babinet, L. G. Moretto, J. Galin, R. Jared, J. Moulton, and L. F. Thompson, Lawrence Berkeley Laboratory Report No. LBL 4080, 1975 (unpublished).

[5]F. Pühlhofer, W. Pfeffer, B. Kohlmeyer, and W. F. W. Schneider, Nucl. Phys. A244, 329 (1975).

[6]J. Dauk, K. P. Lieb, and A. M. Kleinfeld, Nucl. Phys. A241, 170 (1975).

[7]T. M. Cormier, R. S. Galik, E. R. Cosman, and A. J. Lazzarini, Nucl. Instrum. Methods 119, 145 (1974).

[8]T. M. Cormier, E. R. Cosman, A. J. Lazzarini, J. D. Garrett, and H. E. Wegner, Phys. Rev. C 14, 334 (1976).

[9]F. Pühlhofer (unpublished).

[10]H. H. Gutbrod, W. G. Winn, and M. Blann, Nucl. Phys. A213, 267, 285 (1973); and private communication.

[11]D. Wilmore and P. E. Hodgson, Nucl. Phys. 55, 673 (1964); P. E. Hodgson, Annu. Rev. Nucl. Sci. 17, 1 (1967); F. G. Perey, Phys. Rev. 131, 745 (1963); J. R. Huizenga and G. Igo, Nucl. Phys. 29, 462 (1961).

[12]J. R. Grover and J. Gilat, Phys. Rev. 157, 802 (1967).

[13]J. Gilat and J. R. Grover, Phys. Rev. C 3, 734 (1971).

[14]W. Dilg, W. Schantl, and H. Vonach, Nucl. Phys. A217, 269 (1973).

[15]W. D. Myers and W. J. Swiatecki, Nucl. Phys. 81, 1 (1966); Ark. Fys. 36, 343 (1967).

[16]W. D. Myers, Nucl. Phys. A204, 465 (1973).

[17]S. Cohen, F. Plasil, and W. J. Swiatecki, Ann. Phys. 82, 557 (1974).